Supplement of

Variations and sources of volatile organic compounds (VOCs) in urban region: insights from measurements on a tall tower

Xiao-Bing Li[1,2], Bin Yuan[1,2,*], Sihang Wang[1,2], Chunlin Wang[3,4], Jing Lan[3,4], Zhijie Liu[1,2], Yongxin Song[1,2], Xianjun He[1,2], Yibo Huangfu[1,2], Chenglei Pei[5,6,7,8], Peng Cheng[9], Suxia Yang[1,2], Jipeng Qi[1,2], Caihong Wu[1,2], Shan Huang[1,2], Yingchang You[1,2], Ming Chang[1,2], Huadan Zheng[10], Wenda Yang[9], Xuemei Wang[1,2], and Min Shao[1,2]

[1] Institute for Environmental and Climate Research, Jinan University, Guangzhou 511443, China

[2] Guangdong-Hongkong-Macau Joint Laboratory of Collaborative Innovation for Environmental Quality, Guangzhou 511443, China

[3] Guangzhou Climate and Agrometeorology Center, Guangzhou, 511430, China

[4] Southern Marine Science and Engineering Guangdong Laboratory (Zhuhai), Zhuhai, 519082, China

[5] State Key Laboratory of Organic Geochemistry and Guangdong Key Laboratory of Environmental Protection and Resources Utilization, Guangzhou Institute of Geochemistry, Chinese Academy of Sciences, Guangzhou 510640, China

[6] CAS Center for Excellence in Deep Earth Science, Guangzhou, 510640, China

[7] University of Chinese Academy of Sciences, Beijing 100049, China

[8] Guangzhou Ecological and Environmental Monitoring Center of Guangdong Province, Guangzhou 510060, China

[9] Institute of Mass Spectrometer and Atmospheric Environment, Jinan University, Guangzhou 510632, Guangdong, China

[10] Guangdong Provincial Key Laboratory of Optical Fiber Sensing and Communications, and Department of Optoelectronic Engineering, Jinan University, Guangzhou, 510632, China

[*] Corresponding authors: byuan@jnu.edu.cn

Table S1. Average mixing ratio, limits of detection (LOD), and instrument sensitivity for the VOC species reported in this study.

m/z	Chemical Fomular	Suggested Compound	Average mixing ratio (pptv)	LOD** (pptv)	Sensitivity (cps/ppb)
26.015	C2H2	alkyl frag	8.3	4.2	686.8
27.023	C2H3	acetylene, alkyl frag	7.4	4.9	705.3
28.031	C2H4	alkyl frag	6.0	5.2	723.5
31.018	CH2OH	Formaldehyde*	4532.4	12.9	298.1
33.033	CH4OH	Methanol*	8680.0	22.4	466.6
41.039	C3H5	aromatic frag, propyne, methylcyclopentane frag, MBO frag	112.1	9.6	937.1
42.034	C2H3NH	Acetonitrile*	191.8	2.6	1261.6
42.046	C3H6	cyclopentane frag	5.5	1.7	952.0
43.018	C2H2OH	oxygenate frag, ketene	755.6	7.8	1357.3
43.054	C3H6H	alkyl frag, propene, propanol	413.1	6.3	966.8
44.049	C2H5NH	etheneamine	3.5	2.4	1230.1
45.033	C2H4OH	Acetaldehyde*	2535.8	10.0	1356.3
46.029	CH3NOH	formamide[#]	24.4	3.6	1218.1
47.013	CH2O2H	formic acid[#]	749.5	40.8	331.2
47.049	C2H6OH	Ethanol*	15824.2	113.7	197.7
48.044	CH5NOH	hydroxy methyl amine	1.3	0.6	2179.2
49.028	CH4O2H	methane diol, formaldehyde water cluster	6.7	2.1	1435.3
49.011	CH4SH	methane thiol	4.3	1.2	1381.9
51.044	CH6O2H	methanol water cluster	1792.2	7.1	1462.6
51.023	C4H2H	aromatic frag, butadiyne	5.0	3.4	1077.6
51.995	ClH2NH	chloramide	1.9	1.0	1706.6
53.039	C4H4H	Isoprene frag, alkyl frag, butenyne	4.4	2.1	1103.6
54.034	C3H3NH	acrylonitrile	4.6	0.5	2758.4

57.033	C3H4OH	Acrolein*	192.2	13.2	1691.7
57.070	C4H9	butenes, alkyl frag, butanol	798.2	1.0	1204.8
58.029	C2H3NOH	methyl isocyanate, hydroxy acetonitrile	6.0	0.8	2103.9
59.049	C3H6OH	Acetone*	4386.8	6.7	1755.1
60.044	C2H5NOH	acetamide[#]	42.1	2.9	1693.6
61.028	C2H4O2H	Acetic acid[#]	4792.9	34.8	661.5
62.024	CH3NO2H	nitromethane	10.2	1.3	2520.9
63.044	C2H6O2H	ethane diols, acetaldehyde water cluster, ethyl hydroperoxide, ethylene glycol	366.1	5.1	1522.0
65.023	CH4O3H	formic acid water cluster	57.7	3.5	1804.9
65.060	C2H8O2H	ethanol water cluster	1246.2	34.8	1605.2
67.039	CH7O3	methane diol water cluster	2.1	0.7	1821.4
67.054	C5H6H	cyclopentadiene, monoterpene frag	11.3	2.1	1267.6
68.049	C4H5NH	pyrrole[#]	4.3	1.3	1205.7
68.062	C5H8	alkyl frag	4.7	1.4	1278.2
69.055	CH8O3H	methanol +2 water cluster	26.9	1.4	1836.9
69.033	C4H4OH	Fural*	30.5	3.6	1194.0
69.070	C5H8H	Isoprene*	293.7	4.5	1068.7
70.065	C4H7NH	butane nitrile	11.6	1.0	2756.5
71.049	C4H6OH	Methy Vinyl Ketone*	316.5	3.7	1919.5
71.086	C5H10H	pentenes, alkyl frag, C2 and C3 cyclhexanes	271.6	3.9	1308.1
72.044	C3H5NOH	ethyl isocyanate, Methoxyacetonitrile, acrylamide	4.8	0.9	3113.7
72.057	C4H8O	C4 carbonyl O2+ product	11.8	1.3	1552.1
73.028	C3H4O2H	methyl glyoxal,	57.7	2.4	1713.7

		acrylic acid			
73.065	C4H8OH	2-Butanone/Methyl Ethyl Ketone*	1183.9	9.4	1938.2
73.101	C5H12H	pentanes (esp isopentane)	13.3	1.5	1329.2
74.060	C3H7NOH	C3 amides	177.2	2.1	2708.0
75.044	C3H6O2H	Hydroxyacetone*, propionic acid, methyl acetate, ethyl formate	2288.1	14.6	1234.8
75.080	C4H10OH	butanols, monoterpene oxidation product	23.4	2.0	1569.0
76.039	C2H5NO2H	nitroethane	7.4	1.4	2439.2
77.023	C2H4O3H	hydroxy or peroxyacetic acid (PAN indicator), glycolic acid	148.7	2.9	1972.0
77.060	C3H8O2H	acetone water cluster, C3 hydroperoxide, propane diols	200.4	3.0	1678.6
77.039	C6H5	aromatic frag	3.7	1.5	1367.5
78.046	C6H6	benzene charge transfer	8.8	1.2	1376.8
79.039	C2H6O3H	acetic acid water cluster	277.2	5.8	1901.2
79.075	C3H10O2H	propanol water cluster	24.6	1.1	1688.0
79.054	C6H6H	Benzene*	384.7	3.4	1235.1
80.034	CH5NO3H	trihydroxy methyl amine	10.0	2.1	1394.9
80.990	C2H2FClH	chlorofluoroethene	23.4	1.0	1403.8
81.055	C2H8O3H	ethane diol water cluster	12.1	1.7	1911.7
81.033	C5H4OH	cyclopentadiene ketone	4.5	2.1	2483.4
81.070	C6H8H	monoterpene frag,	97.6	2.7	1403.9

		decahydronaphthalene frag			
83.013	C4H2O2H	C4 2-oxy 4-DBE	5.0	1.3	1752.0
83.049	C5H6OH	methyl furan, cyclopentenone, pent-2-ynal	36.8	2.5	1379.5
83.086	C6H10H	hexadienes, methylcyclopentane, cyclohexene, alkene or cycloalkane frag, hexenol and hexanal indicator	185.3	3.4	1421.4
84.081	C5H9NH	C5 nitrile	4.4	0.9	2998.6
84.938	CrO2H	chromium (stainless steel)	7.0	1.4	1709.9
85.028	C4H4O2H	furanone, hydroxy furan	24.6	3.9	1889.3
85.065	C5H8OH	C5 ketones, cyclopentanone, 2ethylacrolein, dihydromethylfuran, dihydropyran, MBO NO+	52.0	2.4	2352.7
85.101	C6H12H	methylcyclopentane, pentenes, cyclohexane	140.0	2.9	1438.4
87.044	C4H6O2H	frag, butadione, methyl acrylate, vinyl acetate, dihydrodioxin, butyrolactone	210.3	4.5	1717.0
87.080	C5H10OH	2-Pentanone*	102.7	2.7	1997.9
88.039	C3H6NO2	acetone NO+ product, nitropropenes, oxazolidone	20.0	1.2	2791.9
88.076	C4H9NOH	C2 acetamides, C4 amides, morpholine	54.1	1.4	2791.9

89.023	C3H4O3H	oxo propanoic (pyruvic) acid, acetic-formic acid anhydride, APAN indicator	5.7	3.5	1946.3
89.060	C4H8O2H	ethyl acetate, butryic acid, hydroxy butanone, acetoin	2773.7	6.6	1059.3
89.096	C5H12OH	pentanols	14.5	1.0	1679.4
91.039	C3H6O3H	hydroxy or peroxypropanoi c acid, PPN indicator	315.8	4.9	2030.7
91.075	C4H10O2H	butane diols, C4 carbonyl water cluster	60.3	1.5	2171.6
91.054	C7H6H	aromatic frag	155.1	4.3	1486.6
92.062	C7H8	toluene charge transfer	62.9	1.7	1494.2
93.055	C3H8O3H	propanoic acid water cluster	104.8	6.6	1959.7
93.091	C4H12O2H	C4 alcohol water cluster	67.8	1.2	1738.2
93.033	C6H4OH	ethyne furan	273.2	14.3	1663.4
93.070	C7H8H	Toluene*	1483.6	1.2	1539.0
95.049	C6H6OH	Phenol*	20.6	3.9	1513.1
95.086	C7H10H	decahydronapht halene frag, monoterpene frag	28.7	2.1	1516.6
96.961	C2H2Cl2H	dichloroethene (uncertain ID)	25.0	1.3	1531.0
97.065	C6H8OH	dimethyl or ethyl furan, hexadienal, methylcyclopent enone, cyclohexeneone	25.7	2.4	1465.8
97.101	C7H12H	methylcyclohex ane frag, urban OA, monoterpene	86.3	2.7	1531.0

		frag, methylcyclohexene			
98.073	C6H10O	C6 carbonyl +1DBE O2+ product	4.2	1.2	1687.0
99.008	C4H2O3H	C4 3-oxy 4DBE: maleic anhydride	17.1	3.2	2049.5
99.044	C5H6O2H	methyl furanone, methanol furan	32.4	3.7	2955.8
99.080	C6H10OH	hexenones, methylcyclopentanone, cyclohexanone	209.9	2.1	2387.0
99.117	C7H14H	methylcyclohexane, dimethylcyclopentane, alkanes frag	25.1	1.8	1513.5
100.039	C4H5NO2H	MVK NO+ product	5.3	1.5	2669.9
100.076	C5H9NOH	C5 alkene amide, butyl isocyanate, C5 hydroxy nitrile	7.4	1.4	2839.8
101.023	C4H4O3H	C4 3-oxy 3DBE	26.9	4.3	2052.8
101.060	C5H8O2H	methyl methacrylate, pentanedione, propenyl ester acetic acid, acetylacetone,ethyl acrylate	201.9	5.2	1675.8
101.096	C6H12OH	Methyl Isobutyl Ketone*	116.6	2.6	1995.6
102.019	C3H3NO3H	oxazolidine dione	3.0	1.5	1565.3
102.055	C4H8NO2	C4 ketones NO+ product, nitro	6.3	0.9	2770.7
102.091	C5H11NOH	C5 amides	6.9	0.9	2845.8
103.039	C4H6O3H	acetic	34.7	3.2	2247.4

103.075	C5H10O2H	anhydride, MPAN and CPAN indicator pentanoic acids, methyl butanonate,propyl acetate	105.4	2.2	1659.9
105.055	C4H8O3H	hydroxy or peroxy butanoic acid (from PiBN or PnBN), various acetic acid ethoxy and methoxy esters	37.9	2.0	2058.0
105.091	C5H12O2H	pentane diols, C5 carbonyl water cluster	12.8	1.5	1817.4
105.033	C7H4OH	C7 1-oxy 6-DBE	24.8	2.2	1741.1
105.070	C8H8H	Styrene*	136.6	2.5	1875.6
106.078	C8H10	C8 aromatics charge transfer	56.6	1.0	1591.0
107.034	C3H6O4H	C3 4-oxy 1-DBE	5.2	1.6	2084.1
107.070	C4H10O3H	C4 acid water cluster	25.5	2.2	1990.2
107.107	C5H14O2H	C5 alcohol water cluster	51.3	1.2	1787.4
107.049	C7H6OH	benzaldehyde	107.8	1.9	2490.6
107.086	C8H10H	C8 aromatics*	1478.3	3.3	1699.3
109.050	C3H8O4H	C3 tetrols	9.1	1.9	2085.7
109.028	C6H4O2H	benzoquinone	9.1	1.7	1924.4
109.101	C8H12H	terpene frag	19.8	1.9	1697.6
111.065	C3H10O4H	propanoic acid +2 water cluster	29.8	3.9	2017.1
111.044	C6H6O2H	methyl furfural, benzene diol, frag[#]	247.3	21.2	695.1
111.080	C7H10OH	C3 substituted furan, biogenic oxidation product, C7 cylcoalkenones	2.9	1.1	1552.5
111.117	C8H14H	C2 and C3	79.8	2.7	1621.1

113.023	C5H4O3H	cyclohexanes frag, biogenic frag, octadiene methylfurandione, biogenic ox product	47.5	3.9	2063.2
113.060	C6H8O2H	dimethylfuranone, methyloxopentanal, biogenic ox product,		3.1	2081.4
		hydroxy methyl cyclohexanone	34.8		
113.096	C7H12OH	ethyl cyclopentanone	34.2	1.7	2398.1
113.132	C8H16H	dimethylcyclohexanes, alkane frag	34.6	2.0	1632.6
114.055	C5H7NO2H	C5 1-nitro, 2-oxy, 3-DBE, C5 ketones +1DBE		1.0	2696.5
		NO+ product	7.2		
115.039	C5H6O3H	C5 3-oxy 3DBE	33.4	3.8	2063.5
115.075	C6H10O2H	C6 diketone isomers, vinylethyl acetate	79.3	3.3	1846.7
115.112	C7H14OH	heptanal, dimethylpetnaone, heptanone	40.4	1.3	2398.0
116.906	CCl3	carbon tet O2+ product	70.6	3.7	1654.7
117.018	C4H4O4H	fumaric acid	5.9	2.7	2088.3
117.055	C5H8O3H	C5 3-oxy 2-DBE isomers,hydroxy ethyl acrylate	23.7	3.4	2063.5
117.091	C6H12O2H	butyl ester acetic acid,diacetonealcohol,butyl acetate	236.2	2.0	1810.7
117.127	C7H16OH	C7 saturated alcohols	5.4	1.0	1777.4

118.050	C4H7NO3H	butene nitrates	8.5	1.8	1659.8
119.034	C4H6O4H	butane dioic acid	10.2	3.1	2088.1
119.107	C6H14O2H	C6 saturated diols, C6 carbonyl water cluster,butoxy ethanol	104.1	1.9	1826.1
119.089	C6H14SH	C6 thiols/sulfides	6.3	1.3	1780.2
120.093	C9H12	C9 aromatics charge transfer	7.1	0.8	1670.1
121.065	C8H8OH	tolualdehyde, acetophenone, dihydrobenzofuran, vinylphenol, benzeneacetaldehyde	64.5	1.8	2395.6
121.101	C9H12H	C9 aromatics*	231.8	2.7	1800.9
122.008	C2H3NO5H	C2H3NO5H+	13.2	1.9	1680.3
123.044	C7H6O2H	salicyladehyde, benzodioxole, benzoic acid	17.8	2.5	2382.2
123.080	C8H10OH	4-ethylphenol, dimethylphenol, methylanisole	4.1	1.1	1797.4
123.117	C9H14H	terpene frag, santene	18.7	1.8	1685.0
124.039	C6H5NO2H	nitrobenzene	2.8	1.1	3081.4
125.060	C7H8O2H	Guaiacol*	10.9	3.0	2670.7
125.132	C9H16H	trimethylcyclohexane frag	51.2	2.2	1694.6
127.075	C7H10O2H	furanone	20.4	3.0	1878.7
127.112	C8H14OH	cyclooctanone	30.6	1.7	2390.3
127.148	C9H18H	trimethylcyclohexane	12.1	1.7	1703.9
129.055	C6H8O3H	methyloxopentenoic acid, acetylmethyloxiranecarbaldehyde	20.9	3.0	2057.5
129.091	C7H12O2H	allyl ester isobutyric acid,butyl	40.4	2.7	1846.4

		acrylate			
129.127	C8H16OH	octanal	39.8	1.8	2388.0
129.070	C10H8H	naphthalene*	34.3	3.3	2284.9
131.034	C5H6O4H	C5 diacid +1DBE	10.7	2.8	2080.8
131.070	C6H10O3H	dimethylfuranone, methyloxopentanal water cluster	22.9	2.4	2055.6
131.107	C7H14O2H	C7 carboxylic acid	13.8	1.7	1708.3
133.086	C6H12O3H	C6 hydroxy or peroxy acid,ethoxyethyl acetate	58.2	1.1	2053.5
133.076	C8H8N2H	Methylpyrrolo[2-a]pyrazine, 1-methylindazole, benzimidazole	4.5	0.8	2470.2
133.101	C10H12H	methyl-tetrahydronaphthalene, butenyl benzene, 2-phenyl 2-butene, ethyl styrene, isopropenyltoluene	28.5	1.4	1730.2
134.109	C10H14	C10 aromatics charge transfer	3.0	0.7	1734.3
135.102	C6H14O3H	C6 acid water cluster	51.6	2.3	2051.4
135.138	C7H18O2H	C7 alcohol water cluster	5.8	1.0	1870.2
135.117	C10H14H	C10 aromatics	153.3	1.7	1738.4
136.022	C7H5NSH	benzothiazole	9.0	2.2	1742.6
137.060	C8H8O2H	phenyl ester of acetic acid, methyl ester of benzoic acid, toluene aromatic acid	14.7	2.2	1867.3
137.132	C10H16H	Monoterpene*	276.0	3.3	902.9
139.042	C4H10O3SH	sulfolane water cluster	3.7	1.7	1754.2

139.039	C7H6O3H	salicylic acid, biogenic ox product, PBzN indicator	5.9	1.4	2047.6
139.112	C9H14OH	nopinone, C5 substituted furan	38.3	1.5	2373.4
139.148	C10H18H	C10 1DBE hydride abstraction	24.8	1.8	1754.0
140.034	C6H5NO3H	benzene nitrophenol, benzene nitrate[#]	15.4	5.4	1526.2
141.127	C9H16OH	C9 carbonyl +1DBE, C9 alcohol +2DBE	15.7	1.3	2370.2
141.164	C10H20H	C10 1DBE, C10 alkanes hydride abstraction	9.6	1.6	1761.5
143.107	C8H14O2H	C8 2-oxy 2DBE isomers	23.3	2.3	1914.4
143.143	C9H18OH	nonanal	87.7	2.0	2367.0
145.122	C8H16O2H	C8 carboxylic acid	22.5	1.9	1714.5
149.117	C7H16O3H	C7 acid water cluster	19.4	1.4	1989.5
149.132	C11H16H	C11 aromatics	26.4	1.2	1789.1
151.112	C10H14OH	pinonaldehyde, C10 aromatic alcohols	13.8	1.4	2004.7
151.148	C11H18H	C11 3-DBE	14.4	1.5	1795.5
153.055	C8H8O3H	methyl salicylate, C8 aromatic hydroxyacid	10.6	1.5	2034.5
153.127	C10H16OH	apinene oxide, camphor, C6 substituted furans	23.8	1.7	1959.9
153.164	C11H20H	C11 2-DBE	11.6	1.5	1801.6
155.143	C10H18OH	linalool, borneol,terpilenol	14.5	1.8	1876.6
155.179	C11H22H	C11 1-DBE, C11 alkanes	8.2	1.4	1807.5

		NO+ product			
157.159	C10H20OH	Menthol-type monoterpenes, decanal	38.0	2.5	1871.0
161.081	C7H12O4H	C7 di-acids	9.8	1.6	2047.7
161.154	C9H20O2H	C9 saturated diols, C9 carbonyl water cluster	13.1	1.3	1945.0
161.132	C12H16H	aromatic frag	3.5	0.8	1824.3
163.133	C8H18O3H	C8 acid water cluster	7.8	1.9	1981.7
163.148	C12H18H	C12 aromatics	7.0	1.4	1829.4
165.164	C12H20H	C12 3-DBE	13.1	1.5	1834.4
167.179	C12H22H	C12 2-DBE	7.6	1.4	1839.2
169.122	C10H16O2H	pinonaldehyde, apinene hydroperoxide	17.1	2.0	1955.8
169.195	C12H24H	C12 1-DBE, alkyl frag	10.1	1.7	1843.8
171.174	C11H22OH	C11 1-oxy 1-DBE	10.0	1.4	1907.1
178.071	C6H11NO5H	C6 1-nitro 5-oxy 2-DBE	2.4	1.0	1863.3
179.179	C13H22H	C13 3-DBE	11.8	1.4	1864.9
C14H10H+	C14H10H	Anthracene or phenanthrene	H3O+ 20.6	2.6	1888.7
181.195	C13H24H	C13 2-DBE	6.4	1.4	1868.6
183.211	C13H26H		6.9	1.5	1872.2
185.190	C12H25O	Dodecanal	8.8	1.6	1910.1
191.179	C14H22H		8.2	2.9	1885.4
193.195	C14H24H		11.4	1.5	1888.4
195.174	C13H22OH	Solanone	2.4	1.1	1919.0
195.211	C14H26H		6.6	1.4	1891.2
197.226	C14H28H		7.3	1.6	1893.9
199.169	C12H22O2H	Menthyl acetate	15.4	1.6	1965.3
203.179	C15H22H		5.0	1.2	1901.7
205.195	C15H24H		23.4	1.7	1904.0
207.211	C15H26H		9.8	1.3	1906.2
209.226	C15H28H	Drimane	5.8	1.3	1908.3
211.242	C15H30H		6.1	1.5	1910.3
215.179	C16H22H		4.7	1.4	1914.4
219.211	C16H26H	Perhydropyrene	6.9	1.6	1917.8

221.226	C16H28H		6.4	1.2	1919.4
223.064	C6H18O3Si3H	D3 Siloxane*	70.1	7.9	1074.9
297.082	C8H24O4Si4H	D4 Siloxane*	41.5	6.8	872.1
299.062	C7H23O5Si4	D5 Siloxane frag	25.7	2.8	1948.9
371.101	C10H30O5Si5H	D5 Siloxane*	15.1	6.7	709.5

* Those VOC species are calibrated using the gas standard.

Those VOC species are calibrated using the Liquid Calibration Unit (LCU).

** LOD of VOC species was derived at the initial time resolution of 10 s.

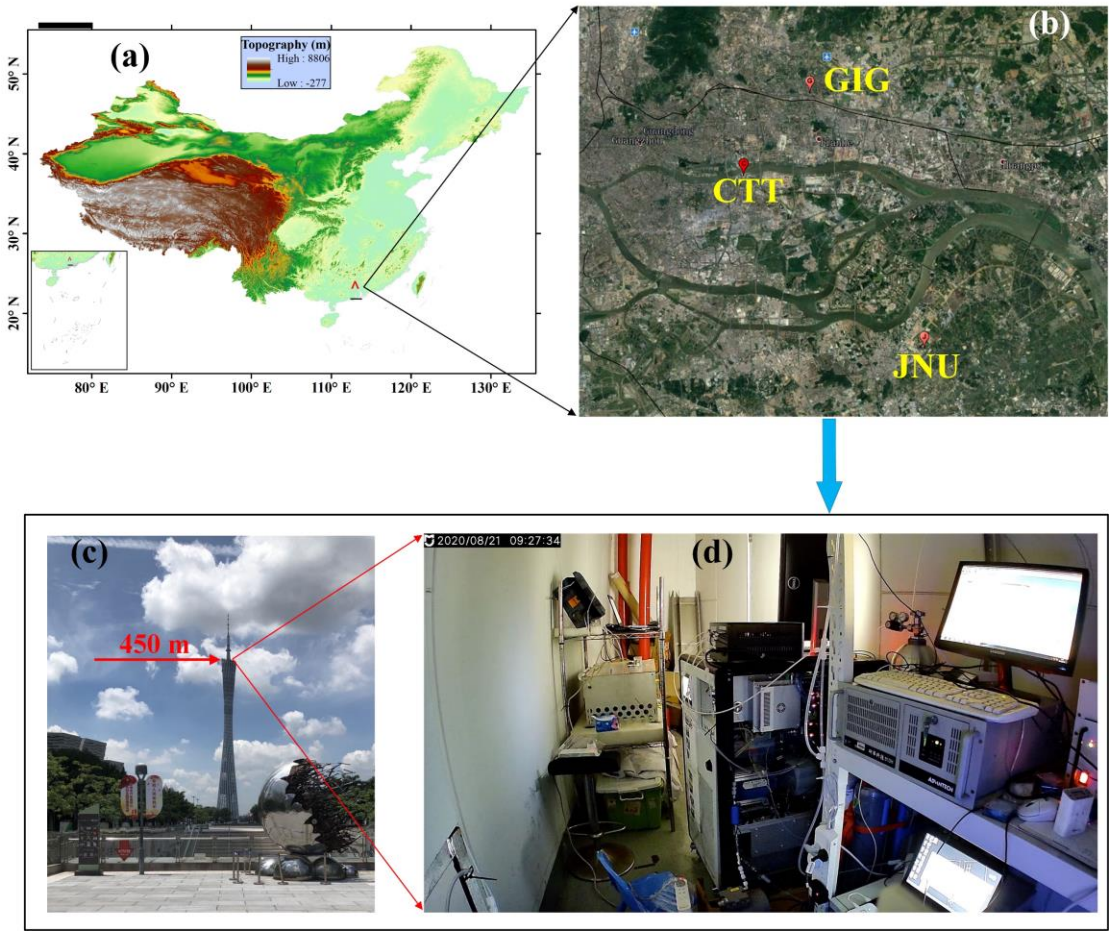

Figure S1. (a) Geographical location of the CTT site in China. (b) Geographical locations of the CTT, GIG, and JNU sites in Guangzhou. (c) Location of the 450 m Look Out platform on the CTT. (d) Picture of the instruments deployed in the observation room at the 450 m Look Out platform. Note that the map in panel (b) is extracted from © Google Maps by the authors.

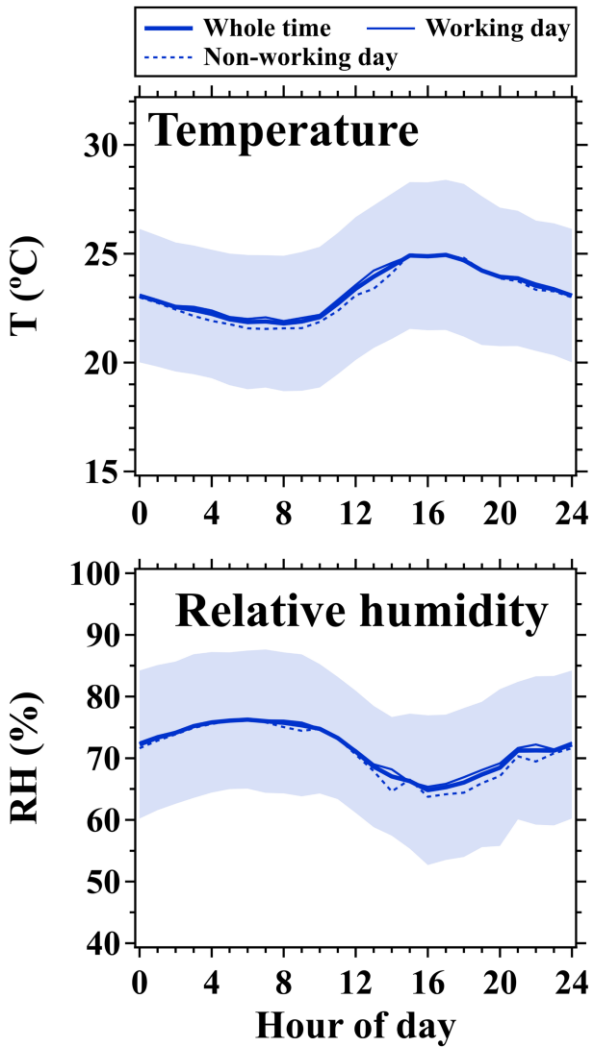

Figure S2. Diurnal variations in temperature (T) and relative humidity (RH) measured at 488 m. Thick blue solid lines and shaded areas represent averages and standard deviations during the CTT campaign (August 18–November 05, 2020); Thin blue solid and dashed lines represent averages on working days and non-working (including weekends and public holidays) days, respectively.

PMF receptor model

As expressed in Eq. (S1), the PMF model is a multivariate factor analysis tool that could decompose a data matrix $\boldsymbol{X}$ into two matrices including the source contribution matrix $\boldsymbol{g}$ and the source profile matrix $\boldsymbol{f}$ (Paatero and Tapper, 1994; Paatero et al., 2014).

$$X_{ij} = \sum_{k=1}^{p} g_{ik} \cdot f_{kj} + e_{ij} \quad \text{(S1)}$$

where i is the number of measured samples during the campaign, j is the number of measured chemical species, p is a user-defined number of sources, and $\boldsymbol{e}$ is the residual matrix. The PMF model is solved by minimizing the objective function Q using the measurement uncertainty matrix $\boldsymbol{U}$ and the residual matrix $\boldsymbol{e}$, as expressed in Eq. (S2),

$$Q = \sum_{i=1}^{n} \sum_{j=1}^{m} [\frac{e_{ij}}{U_{ij}}]^2 \quad \text{(S2)}$$

where n is the number of measured samples and j is the number of chemical species.

In this study, the 10-min mean mixing ratios of VOC species were used in the PMF model. The measurement uncertainty matrix $\boldsymbol{U}$ could be described in Eq. (S3),

$$U_{ij} = \sqrt{(NSR_{ij} \cdot x_{ij})^2 + (p_{1j} \cdot x_{ij})^2 + 2 \cdot \left(p_2 \cdot x_{ij}\right)^2 + LOD^2} \quad \text{(S3)}$$

where NSR_{ij} is the NSR for species j, as expressed in Eq. (S4); p_{1j} was assigned to 15% for the VOC species calibrated by the gas standard and LCU and 50% for the remaining VOC species; p_2 is the uncertainty caused by the utilization of mass flow controller (MFC) and was assigned to 1%. In this study, two MFCs were used in the calibration system: one for the gas standard and the other for the zero-air.

$$NSR_{ij} = \frac{\sqrt{C_{fj} \cdot x_{ij} \cdot t + 2 \cdot B \cdot t}}{C_{fj} \cdot x_{ij} \cdot t} \quad \text{(S4)}$$

where NSR_{ij} is the NSR for the i^{th} sample of species j; C_{fj} and B are the average sensitivity and background signal of species j during the campaign; t is the time resolution (10 min) of VOC concentrations used in PMF.

In this study, a total of 225 chemical species (Table S1) were used in the PMF model to quantitatively analyze contributions of likely sources to the VOCs measurements made during the CTT campaign. VOC species with an SNR ≥ 1, 0.2 < SNR < 1, and SNR<0.2 were categorized as "strong", "weak", and "bad", respectively. The uncertainties of weak VOC species were doubled, while bad species were removed from the analysis. Figure S3 shows the change in $Q/Q_{expected}$ ratio with the increased number of factors in PMF. The $Q/Q_{expected}$ ratio decreased slowly when the number of factors increased from 5 to 6. In addition, profiles of two certain factors were highly correlated when the number of factors exceeded 5, resulting in an excessive decomposition of the VOCs measurements. As shown in Figure S4, the VOCs measurements were well reconstructed by a five-factor solution, which was deemed optimal for the PMF analysis in this study.

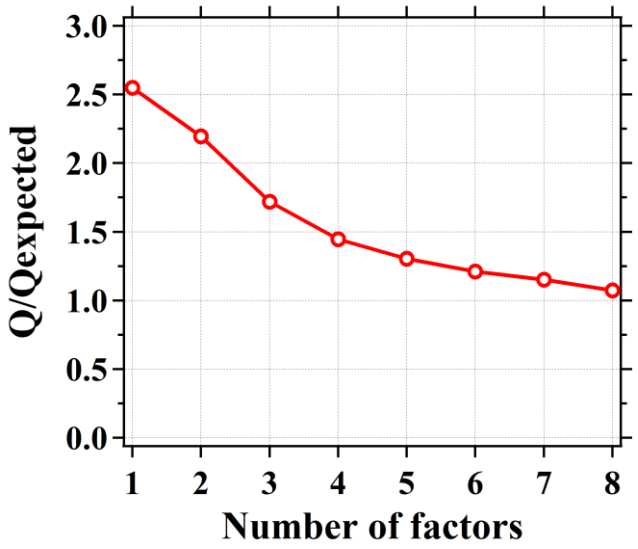

Figure S3. Variation in the ratio of $Q/Q_{expected}$ with change in the number of factors for the PMF analysis.

As shown in Figures 6 and S5, the most prominent composition in factor 1 were OVOC species including acetic acid, formaldehyde, acetone, methanol, acetaldehyde, hydroxyacetone, and formic acid, which contributed to over 70% of the concentration of the factor. These OVOC species with low molecular weights generally have complex sources in urban environments (Hu et al., 2013; Karl et al., 2018; McDonald et al., 2018; Pallavi et al., 2019; Gkatzelis et al., 2021), such as vehicular exhausts, various industrial

processes, biogenic emissions, as well as the oxidative degradation products of hydrocarbons. The diurnal profile of factor 1 increased between LT 09:00–14:00 and continuously decreased from LT 14:00 to 08:00 on the next day, which is consistent with the diurnal variation in ozone. Hourly mean contributions of factor 1 were also well correlated with those of ozone (r=0.75), implying strong dependence of factor 1 on sunlight and temperature. As a result, it is highly challenging to identify sources of factor 1 merely relying on its factor profile that does not contain dominant fingerprint species of specific emission sources. Therefore, factor 1 was assigned to the daytime-mixed source, predominantly including contributions from biogenic emissions and photooxidation products of various VOC species.

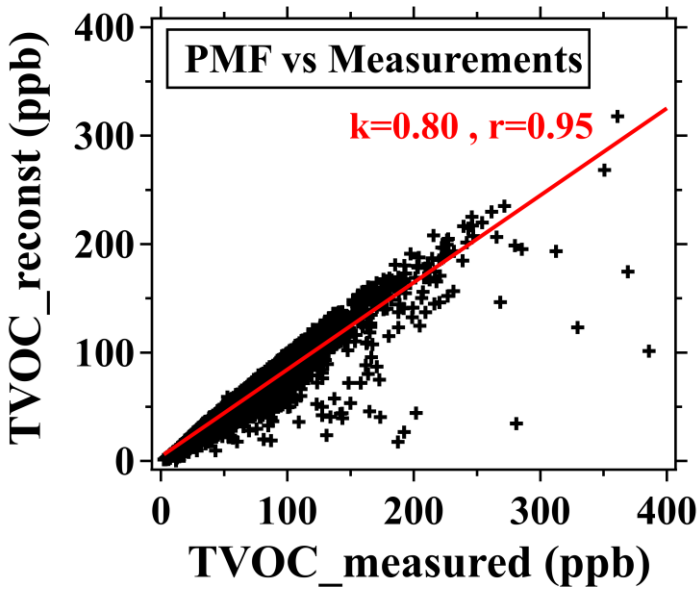

Figure S4. Scatter plots of PMF-reconstructed TVOC concentrations (TVOC_reconst) versus measured TVOC concentrations (TVOC_measured).

Factor 2 was characterized by a high percentage (72%) of ethanol and exhibited a similar diurnal pattern to ethanol. These results confirm that contributions of factor 2 were closely associated with visitor-related emissions. In addition, contributions of factor 2 had the narrowest autocorrelation profile (Figure 6), implying that they were contributed by the most local emission sources. Thus, factor 2 was assigned to the visitor-related source, predominantly including contributions from human breath and volatilization of personal care products. It should be noted that large fractions of ethanol

emitted from personal care products were generally attributed to the VCP source in previous studies (McDonald et al., 2018; Gkatzelis et al., 2021). This is correct when the observation site was not affected by intensive emissions from a known source such as visitors at the 450-m platform. The visitor-related source was resolved in PMF to separate contributions of VCPs from those emitted by visitors.

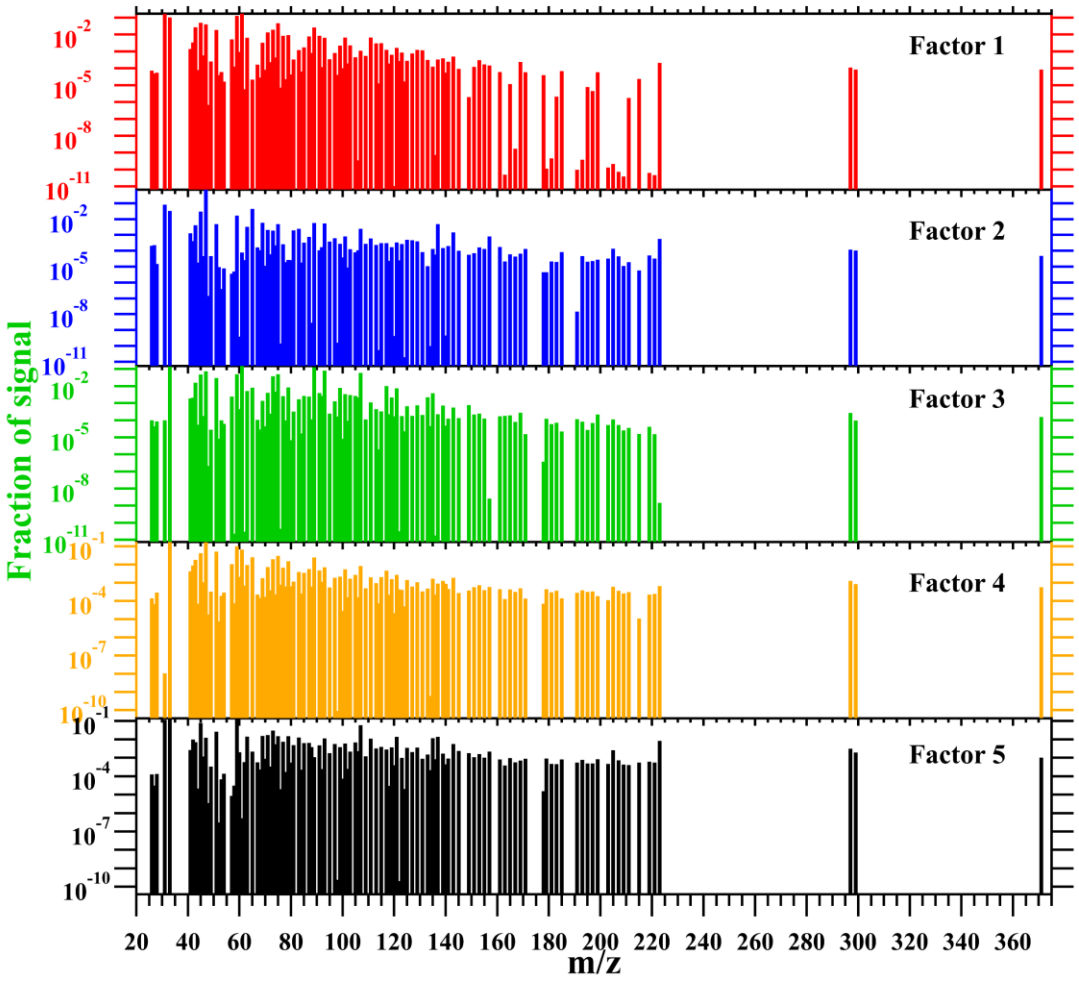

Figure S5. Factor profiles (covering the full range of the mass spectra) of the five factors resolved by the PMF model.

Factor 3 was primarily composed of acetic acid, methanol, ethyl acetate, toluene, ethanol, and C8 aromatics, contributing to over 62% of the concentration of the factor. The diurnal profile of factor 3 was highly consistent with those of aromatics, such as toluene, exhibiting lower mixing ratios during the daytime with a minimum occurring at LT 14:00. Factor 3 explained over 90% and 70% of the variations in toluene and C8 aromatics, respectively, during the campaign. As reported in the literature (Zhang et al.,

2013; Liu et al., 2016; Pallavi et al., 2019), aromatics are known components of vehicular exhausts, solvent usage, industrial raw materials, and emissions of various industrial processes. However, the PMF solution can not explicitly separate these sources in this study due to the lack of measurements for alkanes and low-carbon alkenes. In addition, factor 3 was less affected by visitor-related emissions due to its lower contributions during the opening hours of the 450-m platform on non-working days. Therefore, factor 3 was assigned to the vehicular+industrial source, predominantly including contributions from vehicular exhausts and emissions of various industrial processes.

Methanol, ethanol, acetone, and acetic acid were the most abundant species in factor 4, which contributed to over 51% of the concentration of the factor. The diurnal profile of factor 4 exhibited insignificant variability with slight increases between LT 08:00–13:00. Only a small fraction (<5%) of reactive chemical species such as aromatics were attributed to this factor. Factor 4 was also less affected by visitor-related emissions due to its lower contributions during the opening hours of the 450-m platform on non-working days. To further explore likely sources of factor 4, we also conducted a cluster analysis of 72-h backward trajectories, as detailed in the SI file. As shown in Figure S7, contributions of factor 4 accounted for 13% of the TVOC mixing ratio when affected by continental airflows, but only accounted for 3% when affected by marine airflows. However, contributions of the other factors displayed relatively weaker variations in different clusters of the backward trajectories. These results confirm that contributions of factor 4 had a strong dependence on wind direction and were highly associated with advection transport from nearby or distant cities. In addition, contributions of factor 4 had the flattest autocorrelation profile (Figure 6), indicating that it was less affected by local emissions. Therefore, factor 4 was assigned to the regional transport source, predominantly including contributions from advection transport of aged air masses.

Methanol, acetone, formaldehyde, and acetaldehyde were the most prominent species in factor 5, which contributed to over 46% of the concentration of the factor. In addition to contributions from secondary formation and vehicular exhausts, these

OVOC species were also known components of VCPs (McDonald et al., 2018; Gkatzelis et al., 2021). As shown in Figure 6, the diurnal profile of factor 5 exhibited peak values between LT 08:00–09:00, during which personal care products were extensively used and vehicular exhausts were extensively emitted. Therefore, the diurnal variation pattern of factor 5 was similar to NOx (Figure 4), which is a typical tracer of vehicular exhausts in urban areas. The diurnal profile of factor 5 was also consistent with that of D5-siloxane, which is a key tracer for VCPs in urban environments (Tang et al., 2015; Gkatzelis et al., 2021). As shown in Figure 8, factor 5 contributed to a large fraction (45%) of D5-siloxane and had an ignorable contribution to toluene, confirming predominant contributions of VCPs, rather than vehicular exhausts, in factor 5. Thus, factor 5 was assigned to the VCP-dominated source.

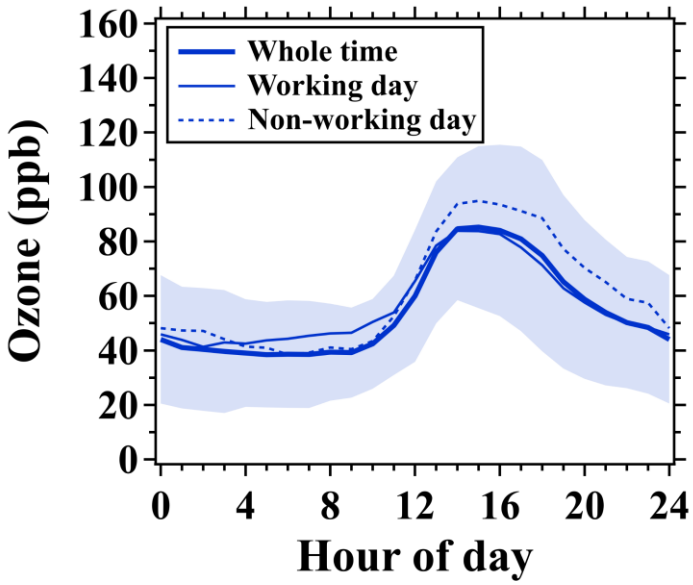

Figure S6. Diurnal variations in ozone mixing ratios measured at 488 m. Thick blue solid lines and shaded areas represent averages and standard deviations during the CTT campaign (August 18–November 05, 2020); Thin blue solid and dashed lines represent averages in working days and non-working (including weekends and public holidays) days, respectively.

Cluster analysis of backward trajectories

Backward trajectories (72 h) of air masses at an arrival altitude of 450 m over the CTT site were calculated for each hour during the campaign using the HYSPLIT Trajectory Model in MeteoInfo software (v 3.0.2). The backward trajectories were calculated based on meteorological data (one-degree resolution, global) from the GDAS system (ftp://ftp.arl.noaa.gov/pub/archives/gdas1) (Stein et al., 2015). Cluster analysis of the backward trajectories was performed in the MeteoInfo software using the Euclidean distance method (Wang, 2014), as shown in Figure S7.

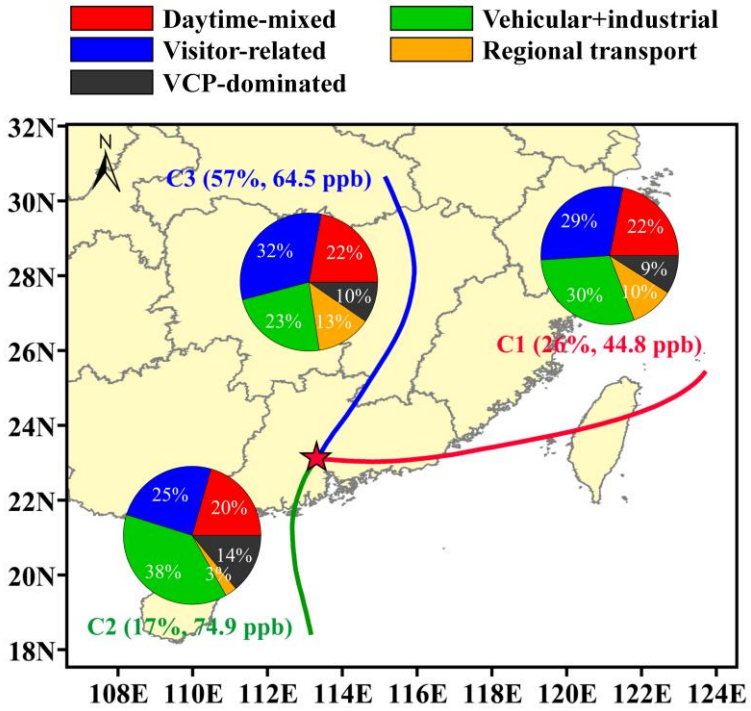

Figure S7. Cluster analysis of 72-h backward trajectories calculated for 24 hours on each day at an arrival altitude of 450 m above ground level at the CTT site. The red star indicates the CTT site. Pie charts indicate the average contributions of the five PMF factors in each cluster. The two digits in each parenthesis refer to the faction of the trajectories and the average TVOC concentration, respectively, in each cluster. C1, C2, and C3 indicate the three clusters of the trajectories, respectively.

Contributions of the five factors displayed strong variations during the campaign. For example, contributions of the visitor-related and regional transport sources

significantly increased from October 3 to November 4, along with prominent decreases in contributions of the vehicular+industrial source. It indicates that contributions of different sources had strong dependences on wind direction. As shown in Figure S7, the three clusters of air masses in this study are similar to those reported in the literature (Xia et al., 2021). Cluster 1, accounting for 26% of the backward trajectories, represents air masses that predominantly originated from the East China Sea and traveled over coastal regions before reaching the CTT site. Cluster 2, accounting for 17% of the backward trajectories, represents air masses that predominantly originated from the South China Sea and traveled over the southwest PRD region before reaching the CTT site. Cluster 3, accounting for 57% of the backward trajectories, represents air masses that predominantly originated from inland regions.

The average TVOC mixing ratios in the three clusters were 44.8, 74.9, and 64.5 ppb, respectively. Cluster 2 was characterized by the highest TVOC mixing ratios during the campaign with the largest contributions (38%) from the vehicular+industrial source. In addition, the regional transport source only contributed to 3% of TVOC mixing ratios in cluster 2 due to the marine origins of air masses. It implies that the measured TVOC mixing ratios were more contributed by local emissions with the higher fractions of reactive VOC species (such as aromatic species) when southwesterly winds prevailed over the PRD region, leading to a frequent occurrence of extremely high ozone mixing ratios. By contrast, contribution fractions of the vehicular+industrial source decreased to 30% and 23% in clusters 1 and 3, respectively, accompanied by significant increases in contributions of the regional transport source. Therefore, transport processes, driven by aged air masses from continental or coastal regions, were also important sources, contributing to over 10% of TVOCs mixing ratios. Contribution fractions of the daytime-mixed source slightly varied in the range of 20–22% among the three clusters of air masses, indicating a weaker wind direction dependence of the daytime-mixed source in comparison to other sources. The VCP-dominated source accounted for the highest fraction (14%) of TVOC mixing ratios in cluster 2 and comparable fractions in clusters 1 (9%) and 3 (10%), further confirming predominant contributions of local anthropogenic emissions when affected by southeasterly air flows.

The visitor-related source contributed to 32% and 29% of TVOC mixing ratios in clusters 1 and 3, respectively, which was significantly greater than in cluster 1. The increased percentages of the visitor-related source in clusters 1 and 3 could be predominantly attributed to reduced contributions from the vehicular+industrial source. In addition, clusters 1 and 3 mainly occurred in the middle and late periods of the campaign, during which the 450-m platform took on more visitors with the successful control of the COVID-19 in China. Therefore, the larger numbers of visitors in clusters 1 and 3 were another important reason for the increased percentages of the visitor-related source in TVOC mixing ratios.

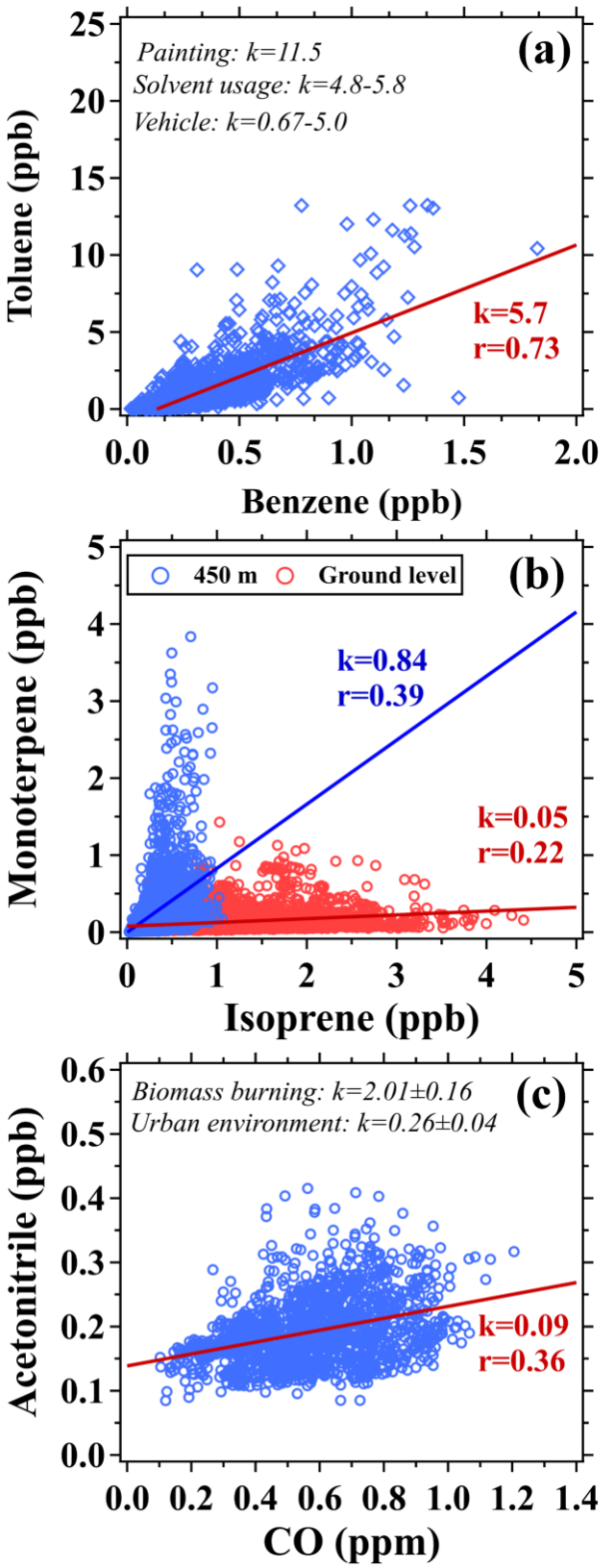

Figure S8. Scatter plots of (a) toluene versus benzene mixing ratios, (b) monoterpene versus isoprene mixing ratios, and (c) acetonitrile versus CO mixing ratios; In panel (b), only the measurements in the daytime (LT 08:00–18:00) were used.

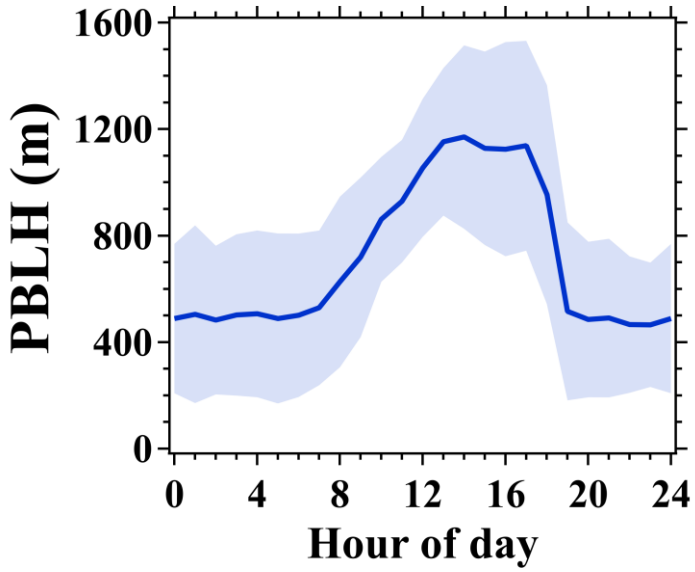

Figure S9. Diurnal variation in planetary boundary layer height (PBLH). Blue solid lines and shaded areas represent averages and standard deviations, respectively.

References

Gkatzelis, G. I., Coggon, M. M., McDonald, B. C., Peischl, J., Gilman, J. B., Aikin, K. C., Robinson, M. A., Canonaco, F., Prevot, A. S. H., Trainer, M., and Warneke, C.: Observations Confirm that Volatile Chemical Products Are a Major Source of Petrochemical Emissions in U.S. Cities, Environ Sci Technol, https://doi.org/10.1021/acs.est.0c05471, 2021.

Hu, L., Millet, D. B., Kim, S. Y., Wells, K. C., Griffis, T. J., Fischer, E. V., Helmig, D., Hueber, J., and Curtis, A. J.: North American acetone sources determined from tall tower measurements and inverse modeling, Atmos. Chem. Phys., 13, 3379-3392, https://doi.org/10.5194/acp-13-3379-2013, 2013.

Karl, T., Striednig, M., Graus, M., Hammerle, A., and Wohlfahrt, G.: Urban flux measurements reveal a large pool of oxygenated volatile organic compound emissions, Proceedings of the National Academy of Sciences of the United States of America, 115, 1186-1191, https://doi.org/10.1073/pnas.1714715115, 2018.

Liu, B., Liang, D., Yang, J., Dai, Q., Bi, X., Feng, Y., Yuan, J., Xiao, Z., Zhang, Y., and Xu, H.: Characterization and source apportionment of volatile organic compounds based on 1-year of observational data in Tianjin, China, Environ Pollut, 218, 757-769, https://doi.org/10.1016/j.envpol.2016.07.072, 2016.

McDonald, B. C., de Gouw, J. A., Gilman, J. B., Jathar, S. H., Akherati, A., Cappa, C. D., Jimenez, J. L., Lee-Taylor, J., Hayes, P. L., McKeen, S. A., Cui, Y. Y., Kim, S.-W., Gentner, D. R., Isaacman-VanWertz, G., Goldstein, A. H., Harley, R. A., Frost, G. J., Roberts, J. M., Ryerson, T. B., and Trainer, M.: Volatile chemical products emerging as largest petrochemical source of urban organic emissions, Science, 359, 760, https://doi.org/10.1126/science.aaq0524, 2018.

Paatero, P., and Tapper, U.: Positive matrix factorization: A non-negative factor model with optimal utilization of error estimates of data values, Environmetrics, 5, 111-126, https://doi.org/10.1002/env.3170050203, 1994.

Paatero, P., Eberly, S., Brown, S. G., and Norris, G. A.: Methods for estimating uncertainty in factor analytic solutions, Atmos. Meas. Tech., 7, 781-797, https://doi.org/10.5194/amt-7-781-2014, 2014.

Pallavi, Sinha, B., and Sinha, V.: Source apportionment of volatile organic compounds in the northwest Indo-Gangetic Plain using a positive matrix factorization model, Atmos. Chem. Phys., 19, 15467-15482, https://doi.org/10.5194/acp-19-15467-2019, 2019.

Stein, A. F., Draxler, R. R., Rolph, G. D., Stunder, B. J. B., Cohen, M. D., and Ngan, F.: NOAA'S HYSPLIT ATMOSPHERIC TRANSPORT AND DISPERSION MODELING SYSTEM, B Am Meteorol Soc, 96, 2059-2077, https://doi.org/10.1175/bams-d-14-00110.1, 2015.

Tang, X., Misztal, P. K., Nazaroff, W. W., and Goldstein, A. H.: Siloxanes Are the Most Abundant Volatile Organic Compound Emitted from Engineering Students in a Classroom, Environmental Science & Technology Letters, 2, 303-307, https://doi.org/10.1021/acs.estlett.5b00256, 2015.

Wang, Y. Q.: MeteoInfo: GIS software for meteorological data visualization and analysis, Meteorol Appl, 21, 360-368, https://doi.org/10.1002/met.1345, 2014.

Xia, S.-Y., Wang, C., Zhu, B., Chen, X., Feng, N., Yu, G.-H., and Huang, X.-F.: Long-term observations of oxygenated volatile organic compounds (OVOCs) in an urban atmosphere in southern China, 2014–2019, Environ Pollut, 270, 116301, https://doi.org/10.1016/j.envpol.2020.116301, 2021.

Zhang, Y., Wang, X., Barletta, B., Simpson, I. J., Blake, D. R., Fu, X., Zhang, Z., He, Q., Liu, T., Zhao, X., and Ding, X.: Source attributions of hazardous aromatic hydrocarbons in urban, suburban and rural areas in the Pearl River Delta (PRD) region, J Hazard Mater, 250-251, 403-411, https://doi.org/10.1016/j.jhazmat.2013.02.023, 2013.